Observation of two multiwave mixing processes via dual optical pumping channels

Shuli Huo (霍淑利), Zhaoyang Zhang (张朝阳), Zhenkun Wu (吴振坤), Huaibin Zheng (郑淮斌), Taikun Liu (刘太昆), Xinxin Xue (薛鑫鑫), Jianping Song (宋建平)*, and Yanpeng Zhang (张彦鹏)**

Key Laboratory for Physical Electronics and Devices of the Ministry of Education and Shaanxi Key Lab of Information Photonic Technique, Xi'an Jiaotong University, Xi'an 710049, China

**Corresponding author: jpsong@mail.xjtu.edu.cn; **corresponding author: ypzhang@mail.xjtu.edu.cn*

Received July 11, 2011; accepted August 15, 2011; posted online November 7, 2011

Based on double optical pumping channels, we experimentally study the competition between two coexistent six-wave mixing (SWM) processes falling into two electromagnetically induced transparency windows by scanning the frequency of the probe field in two similar five-level atomic systems of ^{85}Rb. By blocking one optical pumping channel unrelated to the four-wave mixing (FWM) process, one SWM process, together with the FWM process, generated by a conjugated small-angle static grating could be observed in the spectrum. Moreover, the other SWM process obtained by blocking the first SWM channel is also observed together with the FWM process in a lower N-type four-level subsystem. These experimental results agree well with theoretical predictions.

OCIS codes: 190.4180, 270.1670, 190.4223.
doi: 10.3788/COL201109.121902.

Electromagnetically induced transparency (EIT) has been studied well in the last two decades[1]. Because the generated signals can be transmitted through the resonant atomic medium with little absorption under the EIT condition, multiwave mixing (MWM)[2−4] processes can be investigated. Using one EIT window, the generated four-wave mixing (FWM) and six-wave mixing (SWM) signals are able to coexist in an open-cycle atomic system. Moreover, the competition and interference[5,6] between these FWM and SWM processes have been studied via atomic coherence in a four-level atomic system.

In Fig. 1(a1), the weak probe field E_1 (with tunable frequency ω_1, wave vector $\mathbf{k}_1$, and Rabi frequency G_1) drives the transition from $|0\rangle$ to $|1\rangle$ with resonant wavelength of 780.245 nm. The frequency detuning is Δ_1. The coupling field E_2 (ω_2, $\mathbf{k}_2$, Δ_2, and G_2) drives the transition between $|1\rangle$–$|2\rangle$ with the resonant wavelength of 775.978 nm; two pump beams, E_3 (ω_3, $\mathbf{k}_3$, Δ_3, and G_3) and E_3' (ω_3, $\mathbf{k}_3'$, Δ_3, and G_3'), from the same laser drive the transition between $|3\rangle$–$|4\rangle$ with the resonant wavelength of 780.234 nm, and another pump beam E_4 (ω_4, $\mathbf{k}_4$, Δ_4, and G_4) drives the transition between $|1\rangle$–$|4\rangle$ with the resonant wavelength of 780.235 nm. Using four external cavity diode lasers (ECDL) with line width less than or equal to 1 MHz, these relevant transitions can be effectively driven in ^{85}Rb atoms system. The powers of beams, E_1, E_2, E_3, E_3', and E_4, are 3.7, 50, 20, 20, and 48 mW, respectively. Laser beams E_2, E_3, and E_3' propagate in the same direction with small angles of $\sim 0.3^\circ$ and overlap at one spot inside a rubidium atom vapor cell of 7.5-cm length. A typical atomic density in the cell is 2×10^{11} cm^{-3}. The probe beam E_1 and pump beam E_4 propagate in the same direction (Fig. 1(b)).

According to the phase-matching conditions, one FWM and two SWM processes can be generated simultaneously in the same direction. Firstly, by blocking the coupling beams E_2 and E_4, the FWM process with the phase-matching condition $\mathbf{k}_\mathrm{f} = \mathbf{k}_1 + \mathbf{k}_3 - \mathbf{k}_3'$ can be regarded as a scattering of the probe field E_1 over the small-angle static grating formed by the conjugate field pair of E_3 and E_3'. This FWM process can be further analyzed by Liouville pathway. In Fig. 1(a1), $|4\rangle$ and $|0\rangle$ are hyperfine structures of the ground state; therefore the Liouville pathway of the FWM process is $\rho_{00}^{(0)} \xrightarrow{\omega_3} \rho_{30}^{(1)} \xrightarrow{-\omega_3} \rho_{00}^{(2)} \xrightarrow{\omega_1} \rho_{10}^{(3)}$, which results in the density matrix element $\rho_{10}^{(3)} = -G_\mathrm{A}\exp(\mathrm{i}\mathbf{k}_\mathrm{f}\mathbf{r})/(d_1 d_3 \Gamma_{00})$, where $G_\mathrm{A} = \mathrm{i}G_1 G_3 G_3'^{*}$, $d_1 = \mathrm{i}\Delta_1 + \Gamma_{10}$, $d_3 = \mathrm{i}\Delta_3 + \Gamma_{30}$, and Γ_{ij} are the transverse relaxation rates between states $|i\rangle$ and $|j\rangle$. The atomic coherence can affect the MWM process significantly. The fields related to the generation of FWM signal can affect the FWM signal due to its dressing effect; these are called self-dressing fields[7]. Correspondingly, the effect brought by the coupling beams E_2

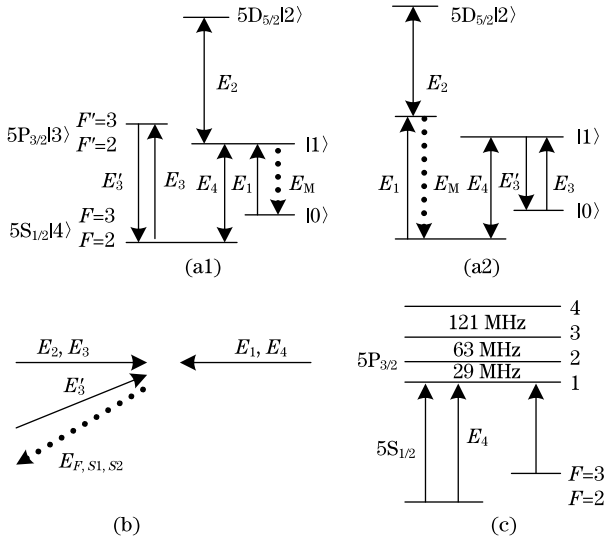

Fig. 1. (a) Five-level atomic system of the ^{85}Rb atom; (b) spatial beam geometry used in the experiment; (c) hyperfine structures of the ^{85}Rb atom corresponding to Fig. 1(a1).

and E_4, as external fields on this FWM process, is denoted as external-dressing effect[8]. Thus, the Liouville pathway of such an external dressed FWM process can be modified as $\rho_{00}^{(0)} \xrightarrow{\omega_3} \rho_{30}^{(1)} \xrightarrow{-\omega_3} \rho_{00}^{(2)} \xrightarrow{\omega_1} \rho_{\pm G_4 \pm G_2 0}^{(3)}$. The above expression becomes $\rho_{10}^{(3)} = -G_{\rm A}\exp(\mathrm{i}\mathbf{k}_{\rm f}\mathbf{r})/[(d_1 + |G_2|^2/d_2 + |G_4|^2/d_4)d_3\Gamma_{00}]$, where $d_2 = \mathrm{i}(\Delta_1 + \Delta_2) + \Gamma_{20}$ and $d_4 = \mathrm{i}(\Delta_1 - \Delta_4) + \Gamma_{40}$. When all incident beams are active except for the pump beam E_4, one can observe the SWM1 process satisfying the phase-matching condition $\mathbf{k}_{\rm s1} = \mathbf{k}_1 + \mathbf{k}_3 - \mathbf{k}_3' + \mathbf{k}_2 - \mathbf{k}_2$ with one photon each from the beams E_1, E_3, E_3', and two photons from the beam E_2. This generated SWM signal falls into an EIT window in a ladder-type three-level subsystem ($|0\rangle - |1\rangle - |2\rangle$) (Fig. 2). Similar to the case of FWM, the Liouville pathway of SWM1 process can be obtained as $\rho_{00}^{(0)} \xrightarrow{\omega_3} \rho_{30}^{(1)} \xrightarrow{-\omega_3} \rho_{00}^{(2)} \xrightarrow{\omega_1} \rho_{10}^{(3)} \xrightarrow{\omega_2} \rho_{20}^{(4)} \xrightarrow{-\omega_2} \rho_{10}^{(5)}$. The density matrix element related to such SWM1 process is $\rho_{10}^{(5)} = G_{\rm B}\exp(\mathrm{i}\mathbf{k}_{\rm s1}\cdot\mathbf{r})/[(d_1)^2 d_2 d_3 \Gamma_{00}]$, with $G_{\rm B} = \mathrm{i}G_1 G_3 G_3'^{*} G_2 G_2^{*}$. When the self-dressing effect of E_2 and external dressing effect of E_4 are considered, the modified Liouville pathway of the SWM1 becomes $\rho_{00}^{(0)} \xrightarrow{\omega_3} \rho_{30}^{(1)} \xrightarrow{-\omega_3} \rho_{00}^{(2)} \xrightarrow{\omega_1} \rho_{\pm G_4 \pm G_2 0}^{(3)} \xrightarrow{\omega_2} \rho_{20}^{(4)} \xrightarrow{-\omega_2} \rho_{\pm G_4 \pm G_2 0}^{(5)}$, and the density matrix element becomes $\rho_{10}^{(5)} = G_{\rm B}\exp(\mathrm{i}\mathbf{k}_{\rm s1}\mathbf{r})/[(d_1 + |G_2|^2/d_2 + |G_4|^2/d_5)^2 d_2 d_3 \Gamma_{00}]$, with $d_5 = \mathrm{i}(\Delta_1 - \Delta_4) + \Gamma_{00}$. Finally, with all incident beams active except for the coupling beam E_2, the second SWM process (SWM2) with phase-matching condition $\mathbf{k}_{\rm s2} = \mathbf{k}_1 + \mathbf{k}_3 - \mathbf{k}_3' + \mathbf{k}_4 - \mathbf{k}_4$ is generated by E_1, E_3, E_3', and E_4. Similarly, the Liouville pathway $\rho_{00}^{(0)} \xrightarrow{\omega_1} \rho_{10}^{(1)} \xrightarrow{-\omega_4} \rho_{40}^{(2)} \xrightarrow{\omega_3} \rho_{30}^{(3)} \xrightarrow{-\omega_3} \rho_{40}^{(4)} \xrightarrow{\omega_4} \rho_{10}^{(5)}$ and the expression $\rho_{10}^{(5)} = G_{\rm C}\exp(\mathrm{i}\mathbf{k}_{\rm s2}\mathbf{r})/[(d_1)^2 (d_4)^2 d_6]$ can be obtained without considering the dressing effect, where $G_{\rm C} = \mathrm{i}G_1 G_3 G_3'^{*} G_4 G_4^{*}$, $d_6 = \mathrm{i}(\Delta_1 - \Delta_4 + \Delta_3) + \Gamma_{40}$. The modified Liouville pathway and density matrix element considering the self-dressing effect of E_4 and external dressing effect of E_2, respectively, are $\rho_{00}^{(0)} \xrightarrow{\omega_1} \rho_{\pm G_4 G_2 0}^{(1)} \xrightarrow{-\omega_4} \rho_{40}^{(2)} \xrightarrow{\omega_3} \rho_{30}^{(3)} \xrightarrow{-\omega_3} \rho_{40}^{(4)} \xrightarrow{\omega_4} \rho_{\pm G_4 G_2 0}^{(5)}$ and $\rho_{10}^{(5)} = G_{\rm C}\exp(\mathrm{i}\mathbf{k}_{\rm s2}\mathbf{r})/[(d_1 + |G_2|^2/d_2 + |G_4|^2/d_4)^2 d_7 (d_4)^2]$, respectively, where $d_7 = \mathrm{i}(\Delta_1 - \Delta_4 + \Delta_3) + \Gamma_{30}$. The MWM signals $E_{\rm F}$, $E_{\rm S1}$, and $E_{\rm S2}$ can be detected along the same direction by an avalanche photodiode detector (APD).

In the experiment, the scan range of Δ_1 is 5 GHz; thus, the information of both $F = 3$ (Fig. 1(a1)) and $F = 2$ (Fig. 1(a2)) can be obtained. In Fig. 1(a2), by changing the current or temperature of the corresponding ECDL, the wavelength of the E_1 tunes to 780.234 nm and the wavelength of the E_3 beam to 780.245 nm to achieve different optical pumping process. Similar to the system shown in Fig. 1(a1), MWM processes ($E_{\rm f}$, $E_{\rm s1}$, and $E_{\rm s2}$) in Fig. 1(a2) also satisfy the phase-matching conditions $\mathbf{k}_{\rm f}' = \mathbf{k}_1 + \mathbf{k}_3 - \mathbf{k}_3'$, $\mathbf{k}_{\rm s1}' = \mathbf{k}_1 + \mathbf{k}_3 - \mathbf{k}_3' + \mathbf{k}_2 - \mathbf{k}_2$, and $\mathbf{k}_{\rm s2}' = \mathbf{k}_1 + \mathbf{k}_3 - \mathbf{k}_3' + \mathbf{k}_4 - \mathbf{k}_4$, respectively. Based on the method in the first atomic system, the following detailed theoretical analyses are obtained as

(1) Undressed FWM process:

$$\rho_{00}^{(0)} \xrightarrow{\omega_3} \rho_{10}^{(1)} \xrightarrow{-\omega_3} \rho_{00}^{(2)} \xrightarrow{\omega_1} \rho_{30}^{(3)},$$

$$\rho_{30}^{(3)} = -G_{\rm A}\exp(\mathrm{i}\mathbf{k}_{\rm f}\mathbf{r})/(d_8 d_9 \Gamma_{00}),$$

where $d_8 = \Gamma_{30} + \mathrm{i}\Delta_1$, $d_9 = \Gamma_{10} + \mathrm{i}\Delta_3$.

Dressed FWM process:

$$\rho_{00}^{(0)} \xrightarrow{\omega_3} \rho_{\pm G_4 0}^{(1)} \xrightarrow{-\omega_3} \rho_{00}^{(2)} \xrightarrow{\omega_1} \rho_{\pm G_2 0}^{(3)},$$

$$\rho_{30}^{(3)} = -G_{\rm A}\exp(\mathrm{i}\mathbf{k}_{\rm f}\mathbf{r})/[(d_8 + |G_2|^2/d_2 + |G_4|^2/d_{10})(d_9 + |G_4|^2/d_{11})\Gamma_{00}],$$

where $d_{10} = \mathrm{i}(\Delta_1 - \Delta_4) + \Gamma_{31}$, $d_{11} = \mathrm{i}(\Delta_3 - \Delta_4) + \Gamma_{00}$.

(2) Undressed SWM1 process:

$$\rho_{00}^{(0)} \xrightarrow{\omega_3} \rho_{10}^{(1)} \xrightarrow{-\omega_3} \rho_{00}^{(2)} \xrightarrow{\omega_1} \rho_{30}^{(3)} \xrightarrow{\omega_2} \rho_{20}^{(4)} \xrightarrow{-\omega_2} \rho_{30}^{(5)},$$

$$\rho_{30}^{(5)} = G_{\rm B}\exp(\mathrm{i}\mathbf{k}_{\rm s1}\mathbf{r})/[(d_8)^2 d_2 d_9 \Gamma_{00}].$$

Dressed SWM1 process:

$$\rho_{00}^{(0)} \xrightarrow{\omega_3} \rho_{\pm G_4 0}^{(1)} \xrightarrow{-\omega_3} \rho_{00}^{(2)} \xrightarrow{\omega_1} \rho_{\pm G_2 0}^{(3)} \xrightarrow{\omega_2} \rho_{20}^{(4)} \xrightarrow{-\omega_2} \rho_{\pm G_2 0}^{(5)},$$

$$\rho_{10}^{(5)} = G_{\rm B}\exp(\mathrm{i}\mathbf{k}_{\rm s1}\mathbf{r})/[(d_8 + |G_2|^2/d_2 + |G_4|^2/d_{10})^2 \cdot d_2 (d_9 + |G_4|^2/d_{11})\Gamma_{00}].$$

(3) SWM2 process:

With the main one in six alternative pathways, the undressed-SWM2 process can be addressed as

$$\rho_{44}^{(0)} \xrightarrow{\omega_4} \rho_{14}^{(1)} \xrightarrow{-\omega_3} \rho_{04}^{(2)} \xrightarrow{\omega_3} \rho_{14}^{(3)} \xrightarrow{-\omega_4} \rho_{44}^{(4)} \xrightarrow{\omega_1} \rho_{34}^{(5)},$$

$$\rho_{34}^{(5)} = G_{\rm C}\exp(\mathrm{i}\mathbf{k}_{\rm s2}\mathbf{r})/[d_{12} d_{13} (d_{14})^2 \Gamma_{44}],$$

where $d_{12} = \mathrm{i}\Delta_1 + \Gamma_{34}$, $d_{13} = \mathrm{i}(\Delta_4 - \Delta_3) + \Gamma_{04}$, and $d_{14} = \mathrm{i}\Delta_4 + \Gamma_{14}$.

The dressed SWM1 process can be addressed as

$$\rho_{44}^{(0)} \xrightarrow{\omega_4} \rho_{1\pm G_4}^{(1)} \xrightarrow{-\omega_3} \rho_{0\pm G_4}^{(2)} \xrightarrow{\omega_3} \rho_{1\pm G_4}^{(3)} \xrightarrow{-\omega_4} \rho_{\pm G_4 \pm G_4}^{(4)} \xrightarrow{\omega_1} \rho_{\pm G_2 \pm G_4}^{(5)},$$

$$\rho_{34}^{(5)} = G_{\rm C}\exp(\mathrm{i}\mathbf{k}_{\rm s2}\mathbf{r})/[(d_{12} + |G_2|^2/d_{15} + |G_4|^2/d_{10}) d_{13}(d_{14} + |G_4|^2/\Gamma_{44}^2)],$$

where $d_{15} = \mathrm{i}(\Delta_1 + \Delta_2) + \Gamma_{24}$. From the expressions listed above, clearly, although the structures of the two energy levels are similar, the influences the coupled fields $\mathbf{k}_3$ and $\mathbf{k}_4$ produce on the different SWM signals are quite different.

Figures 2(a) and (b) show the results of blocking different coupling beams in the first five-level atomic system shown in Fig. 1(a1). The upper curve of Fig. 2(a1) shows the FWM signal when the beams E_1, E_3, and E_3' are active; and the detuning of E_3 is Δ_3=–500 MHz. The FWM signal is not conspicuous because the EIT window is absent due to the Doppler effect in the lower curve of Fig. 2(a1). Hence, the optical pumping is very weak. In Fig. 2(a2), when E_2 is turned on and E_4 is blocked, SWM1 signal shown by the upper curve is generated and falls into the $|0\rangle - |1\rangle - |2\rangle$ ladder-type EIT window shown by the lower curve. Figure 2(a3) shows the experimental results when E_4 is activated and E_2 is blocked. Here, the SWM2 ($\mathbf{k}_{\rm s2}$) signal

shown by the upper curve is generated and falls into the $|0\rangle - |1\rangle - |4\rangle$ Λ-type EIT window, which is shown by the lower curve. More importantly, two sharply enhanced absorption dips are near the SWM signal peak shown in the upper curve of Figs. 2(a3) or (b3), this can be well interpreted by introducing the hyperfine structure of ^{85}Rb, as shown in Fig. 1(c). According to the transition rule in Fig. 1(c), the absorption enhancement in the $^{85}\mathrm{Rb}\,|5\mathrm{S}_{1/2}, F=2\rangle$ dip (the upper curve of Fig. 2(a3)) is due to the leakage of the probe transmission, which have contributions from E_3, E_3', E_4 optical pumping of population from the ground-state $|5\mathrm{S}_{1/2}, F=2\rangle$, as shown in Fig. 2(a3). Hence, the distance between the two dips is 121 MHz, corresponding to that between $|5\mathrm{P}_{3/2}, F=3\rangle$ and $|5\mathrm{P}_{3/2}, F=4\rangle$. When all beams are active, SWM1 ($\mathbf{k}_{\mathrm{s1}}$), SWM2 ($\mathbf{k}_{\mathrm{s2}}$), and FWM ($\mathbf{k}_{\mathrm{f}}$) are generated simultaneously with corresponding EIT windows, as shown in Fig. 2(a4). Similarly, two sharply enhanced absorption dips are apparent in Fig. 2(a4).

The experimental results when the detuning is set at Δ_3=–700 MHz are shown in Figs. 2(b1)–(b4). The meaning of the signal curves in Figs. 2(b1)–(b4) is the same as in Figs. 2(a1)–(a4). Similarly, FWM signal ($\mathbf{k}_{\mathrm{f}}$) in Fig. 2(b1) is not conspicuous because there no EIT window exists. Because of the optical pumping effect corresponding to the transitions from the hyperfine levels $^{85}\mathrm{Rb}\,|5\mathrm{S}_{1/2}, F=2\rangle$ to $|5\mathrm{P}_{3/2}, F=1,2,3\rangle$, the generated SWM1 signal ($\mathbf{k}_{\mathrm{s1}}$) (Δ_3=–500 MHz is slightly stronger than the SWM1 signal ($\mathbf{k}_{\mathrm{s1}}$) (Δ_3=–700 MHz). This phenomenon can be identified in the upper curves of Figs. 2(a2) and (b2). When SWM2 is generated, similarly, two sharply enhanced absorption dips are present because of the effect of optical pumping in Figs. 2(b3) and (b4).

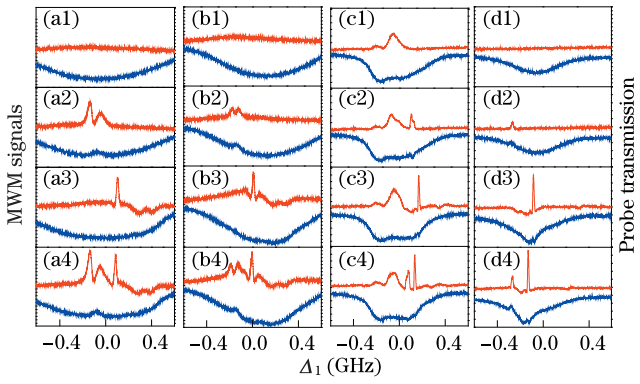

Fig. 2. (Color online) (a) and (b) evolution of the interaction between the EIT (blue curves) windows or MWM (red curves) signals in the atomic system shown in Fig. 1(a1); (c) and (d) evolution of the interaction between EIT (blue curves) windows or MWM (red curves) signals in the atomic system shown in Fig. 1(a2). Specifically, (a1)–(d1) represent FWM signals with E_2 and E_4 blocked; (a2)–(d2) represent SWM1 with E_4 blocked; (a3)–(d3) show SWM2 with E_2 blocked; (a4)–(d4) show coexisting SWM1 and SWM2 when all the beams are on. The parameters are (a1)–(a4): $\Delta_2 = -92$ MHz, $\Delta_4 = 110$ MHz $\Delta_3 = -500$ MHz; (b1)–(b4): $\Delta_2 = 155$ MHz, $\Delta_4 = 0$ MHz, $\Delta_3 = -700$ MHz; (c1)–(c4): $\Delta_2 = -109$ MHz, $\Delta_4 = 169$ MHz, $\Delta_3 = 61.8$ MHz; (d1)–(d4): $\Delta_2 = 269$ MHz, $\Delta_4 = -85$ MHz, $\Delta_3 = -700$ MHz. Other parameters are $G_1 = 4.6$ MHz, $G_2 = 50$ MHz, $G_3 = G_3' = 20$ MHz, $G_4 = 30$ MHz.

Next, we move from the first five-level atomic system shown in Fig. 1(a1) to the second similar five-level atomic system by tuning the wavelength of beams E_1 and E_3, as shown in Fig. 1(a2). Figures 2(c) and (d) show the results of blocking different coupling beams in the second system, as well as the significant differences from those in Figs. 2(a) and (b). When the beams E_1, E_3, and E_3' are all active, the upper curve of Fig. 2(c1) shows that the FWM signal ($\mathbf{k}_{\mathrm{f}}'$) is clearly Doppler-broadened due to the strong optical pumping (Δ_3= 61.8 MHz). In Fig. 2(c2), when E_2 is activated, the SWM1 ($\mathbf{k}_{\mathrm{s1}}'$) shown by the upper curve is generated and falls into the $|4\rangle - |3\rangle - |2\rangle$ ladder-type EIT windows shown by the lower curve. Figure 2(c3) shows the experimental results when E_4 is activated and E_2 is blocked. Here, the generated SWM2 signal ($\mathbf{k}_{\mathrm{s2}}'$) shown by the upper curve falls into the $|4\rangle - |3\rangle - |1\rangle$ V-type EIT window shown by the lower curve. However, the SWM2 process comprises six detailed Liouville pathways. Meanwhile, the absorption increases in the $^{85}\mathrm{Rb}\,|5\mathrm{S}_{1/2}, F=3\rangle$ dip, which has contributions from the E_3 and E_3' optical pumping of population from $|5\mathrm{S}_{1/2}, F=3\rangle$. Absorption decreases in the $^{85}\mathrm{Rb}\,|5\mathrm{S}_{1/2}, F=2\rangle$ dip also appear because of the leakage of probe transmission, which has a contribution from the E_4 optical pumping of population from the ground-state $|5\mathrm{S}_{1/2}, F=2\rangle$. Hence, these contributions from the optical pumping of pump beams E_3, E_3', and E_4 can come to a balance, and there no absorption dips are produced (Figs. 2(c3)–(c4)).

Figure 2(d) shows the results with the detuning of Δ_3=–700 MHz. The FWM signal ($\mathbf{k}_{\mathrm{f}}'$) in upper curve of Fig. 2(d1) is less obvious because no EIT window is present in the lower curve. A comparison of the coexistent FWM signals ($\mathbf{k}_{\mathrm{f}}'$) and SWM signals ($\mathbf{k}_{\mathrm{s1}}'$, $\mathbf{k}_{\mathrm{s2}}'$) in Figs. 2(d1)–(d4) with those in Figs. 2(c1)–(c4) shows that the intensities of FWM ($\mathbf{k}_{\mathrm{f}}'$) and SWM signals ($\mathbf{k}_{\mathrm{s1}}'$, $\mathbf{k}_{\mathrm{s2}}'$) at Δ_3=–700 MHz are smaller than those at Δ_3= 61.8 MHz. No absorption dips are produced for the same reason as that in Figs. 2(c).

Now, we focus on the interplay between the two coexistent SWM signals by varying the frequency detuning of the coupling field E_2 when all five laser beams (E_1, E_2, E_3, E_3', and E_4) are active. The experimental results with the two EIT windows overlapping or separating under four different situations and corresponding to those in previous experiments are shown in Fig. 3. For the first five-level atomic system shown in Fig. 1(a1), a ladder-type EIT window and Λ-type EIT window can coexist. The FWM ($\mathbf{k}_{\mathrm{f}}$) and SWM signals ($\mathbf{k}_{\mathrm{s1}}$, $\mathbf{k}_{\mathrm{s2}}$) can be controlled to overlap or separate by varying the frequency detuning of the coupling beam E_2. The upper curves in Fig. 3 show the interplay and competition between two coexistent SWM processes. In Figs. 3(a1)–(a5) and 3(b1)–(b5), two generated SWM signals can be observed by blocking different laser beams and scanning the probe detuning Δ_1. In Figs. 3(a1)–(a5), when the frequency of E_2 is changed from –192 to 176 MHz, two EIT windows begin to overlap, whereas two SWM signals ($\mathbf{k}_{\mathrm{s1}}$, $\mathbf{k}_{\mathrm{s2}}$) begin to compete. When the SWM2 signal ($\mathbf{k}_{\mathrm{s2}}$) and the right peak of SWM1 signal ($\mathbf{k}_{\mathrm{s1}}$) overlap, an enhancement for the SWM2 signal ($\mathbf{k}_{\mathrm{s2}}$) at the resonance $\Delta_1 + \Delta_2 - G_2 = 0$ (from the dressing field E_2) and a suppression for the SWM1 signal ($\mathbf{k}_{\mathrm{s1}}$) at the resonance

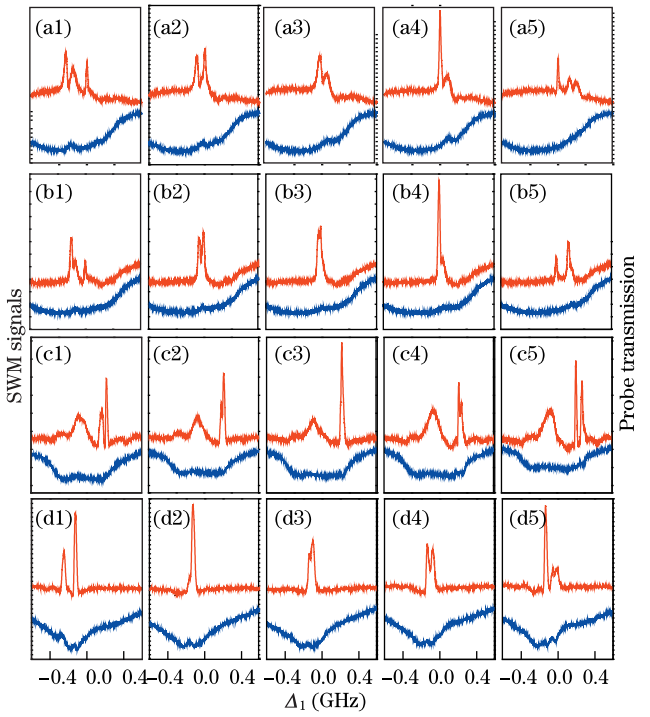

Fig. 3. (Color online) (a) and (b) Evolution of the interplay between two coexistent MWM signals of the atomic system shown in Fig. 1(a1); (c) and (d) evolution of the interplay between two coexistent MWM signals of the system shown in Fig. 1(a2). In each panel, the upper curves show the MWM signals and the lower curves show the probe transmission signals. The experimental condition is the same as that in Figs. 2. (a1)–(a4): $\Delta_2 = -192, -52, 10, 47, 176$ MHz, gradually. (b1)–(b4): $\Delta_2 = -123, -23, -15, 33, 141$ MHz, gradually. (c1)–(c4): $\Delta_2 = -30, -15, -10, 10, 28$ MHz, gradually. (d1)–(d4): $\Delta_2 = -96, -49, -41, -34, 0$ MHz, gradually. Other parameters are $G_1 = 4.6$ MHz, $G_2 = 50$ MHz, $G_3 = G_3' = 20$ MHz, and $G_4 = 30$ MHz.

$\Delta_1 - \Delta_4 = 0$ (from another dressing field E_4) occur, respectively. The total influence between these two SWM signals ($\mathbf{k}_{s1}$, $\mathbf{k}_{s2}$) depends on the competition between the enhancement and suppression. As Fig. 3(a2) shown, because the suppression for SWM1 ($\mathbf{k}_{s1}$) is stronger than the enhancement caused by SWM2 ($\mathbf{k}_{s2}$), the final influence is suppression. When the SWM2 signal ($\mathbf{k}_{s2}$) and the middle dip of SWM1 signal ($\mathbf{k}_{s1}$) overlap, these two modified SWM signal intensities show the suppression at exact resonances $\Delta_1 - \Delta_4 = 0$ (from the dressing field E_4) and $\Delta_1 + \Delta_2 = 0$ (from another dressing field E_2), respectively; the final influence is suppression (Fig. 3(a3)). When the SWM2 signal ($\mathbf{k}_{s2}$) and the left peak of SWM1 signal ($\mathbf{k}_{s1}$) overlap, an enhancement for the SWM2 signal ($\mathbf{k}_{s2}$) at the resonance $\Delta_1 + \Delta_2 + G_2 = 0$ (from the dressing field E_2) and a suppression for the SWM1 signal ($\mathbf{k}_{s1}$) at the resonance $\Delta_1 - \Delta_4 = 0$(from another dressing field E_4) occur, respectively. As Fig. 3(a4) shown, the total influence brought by these two dressed SWM signals is enhancement. When the two EIT windows begin to separate, the interaction between these two SWM signals ($\mathbf{k}_{s1}$, $\mathbf{k}_{s2}$) diminishes. Figures 3(b1)–(b5) (Δ_3= –700 MHz), where the frequency of E_2 is changed from –123 to 141 MHz, show that when SWM2 signal ($\mathbf{k}_{s2}$) and the right or left peak of SWM1 signal ($\mathbf{k}_{s1}$) overlap, a phenomenon similar to that in Figs. 3(a2) and (a4) occurs. When the SWM2 signal ($\mathbf{k}_{s2}$) and the middle dip of SWM1 signal ($\mathbf{k}_{s1}$) overlap, the condition of suppression is the same as that in Fig. 3(a3) for both two SWM signals ($\mathbf{k}_{s1}$, $\mathbf{k}_{s2}$). Here, the suppression in Fig. 3(b3) is weaker than that in Fig. 3(a3).

Figures 3(c1)–(c4) and (d1)–(d4) show the interplay between SWM signals ($\mathbf{k}'_{s1}$, $\mathbf{k}'_{s2}$) in another energy level system shown in Fig. 1(a2). Figures 3(c1)–(c4) (Δ_3= 61.8 MHz) show that, because there is only one peak in the SWM signals ($\mathbf{k}'_{s1}$, $\mathbf{k}'_{s2}$), by changing the frequency of E_2 from –30 to 28 MHz, when SWM2 signal ($\mathbf{k}'_{s2}$) and the left or right side of SWM1 signal peak ($\mathbf{k}'_{s1}$) overlap, there is a suppression for SWM1 signal ($\mathbf{k}'_{s1}$) at exact resonance $\Delta_1 - \Delta_4 = 0$ (from the dressing field E_4) and an enhancement for SWM2 signal ($\mathbf{k}'_{s2}$) at exact resonances $\Delta_1 + \Delta_2 \pm G_2 = 0$ (from another dressing field E_2). As shown in Figs. 3(c2) and (c4), the total influence between these two SWM signals is suppression. However, when SWM2 signal ($\mathbf{k}'_{s2}$) and SWM1 signal ($\mathbf{k}'_{s1}$) overlap completely, there exist suppressions for both the SWM signals ($\mathbf{k}'_{s1}$, $\mathbf{k}'_{s2}$) [Fig. 3(c3)] at exact resonances $\Delta_1 - \Delta_4 = 0$ (from the dressing field E_4) and $\Delta_1 + \Delta_2 = 0$ (from another dressing field E_2). Here, because optical pumping is stronger, the final influence is weak suppression. In Figs. 3(d1)–(d4) (Δ_3= –700 MHz), the frequency of E_2 is changed from –96 to 0 MHz. When SWM2 signal ($\mathbf{k}_{s2}$) and the right or left side of SWM1 signal ($\mathbf{k}_{s1}$) overlap, a phenomenon similar to that shown in Figs. 3(c2) and (c4) is obtained. When the SWM2 ($\mathbf{k}'_{s2}$) and SWM1 signals ($\mathbf{k}'_{s1}$) overlap completely, two suppressions for both the SWM signals ($\mathbf{k}'_{s1}$, $\mathbf{k}'_{s2}$) at the exact resonances $\Delta_1 - \Delta_4 = 0$ (from the dressing field E_4) and $\Delta_1 + \Delta_2 = 0$ (from the dressing field E_2), respectively, exist. As shown in Fig. 3(d3), the final influence is suppression.

This work was supported by the National Natural Science Foundation of China (Nos. 10974151, 61078002, and 61078020), the New Century Excellent Talent Project of the Ministry of Education of China (No. 08-0431), and the Cross-disciplinary Project of Xi'an Jiaotong University (Nos. XJJ20100100 and XJJ20100151).

References

1. S. E. Harris, Phys. Today **50,** 36 (1997).
2. P. R. Hemmer, D. P. Katz, J. Donoghue, M. Cronin-Golomb, M. S. Shahriar, and P. Kumar, Opt. Lett. **20,** 982 (1995).
3. Y. Li and M. Xiao, Phys. Rev. A **51,** 4959 (1995).
4. Y. Wu and L. Deng, Phys. Rev. Lett. **93,** 143904 (2004).
5. Y.-P. Zhang, U. Khadka, B. Anderson, and M. Xiao, Phys. Rev. Lett. **102,** 013601 (2009).
6. Y.-P. Zhang, B. Anderson, A. W. Brown, and M. Xiao, Appl. Phys. Lett. **91,** 061113 (2007).
7. J. Song, Y. Feng, C. Gan, L. Li, Y. Yu, H. Ge, R. Ma, C. Li, X. Zhang, Y. Zhang, and K. Lu, Chin. Opt. Lett. **3,** 283 (2005).
8. C. Zuo, Y. Du, T. Jiang, Z. Nie, Y. Zhang, H. Zheng, C. Gan, W. Zhang, and K. Lu, Chin. Opt. Lett. **6,** 685 (2008).